# ON WAVE TRANSMISSION AT SUBMERGED RUBBLE-MOUND BREAKWATERS WITH LARGE TIDAL RANGE

Elisa Leone[1], Alberica Brancasi[1], Francesco Ciardulli[2], Antonio Francone[1], Sigurdur Sigurdarson[3], Giuseppe R. Tomasicchio[1], Nobuhisa Kobayashi[4] and Giancarlo Chiaia[5]

The present paper provides the results of an experimental and numerical investigation on a submerged rubble-mound breakwater with the aim to study its performance in terms of wave transmission in condition of large tidal range. The experimental investigation has been conducted at the EUMER laboratory of the University of Salento. In the 2D wave flume, a small-scale physical model of a submerged breakwater has been constructed and exposed to different wave conditions and water levels. The experimental observations have been used to calibrate the numerical model CSHORE and to investigate the fraction of the different energy dissipative contributions due to wave breaking, to bottom friction and to porous mound. Additional tests have been numerically conducted to cover a wider range of wave conditions and water levels, allowing to better evaluate the behavior of the submerged rubble-mound breakwater in condition of large tidal range.

*Keywords: submerged rubble-mound breakwater; wave transmission; tidal range*

## INTRODUCTION

Submerged rubble-mound breakwaters (SBW) are coastal defence structures composed of units of different materials with varying shapes and sizes. They are typically adopted in areas with small and moderate tidal ranges to reduce energy of the wave attacks approaching the coast by inducing wave energy dissipation, thus preventing beach erosion and flooding (Calabrese et al. 2002). At present, the performance of this type of coastal defence structures appears to be well known in seas such as the Mediterranean and, in general, where tidal ranges over a day are moderate. In recent years, a variety of experiments have been conducted at various test facilities under different wave conditions, at both small and large scale. These experiments have included rubble-mound structures with permeable natural (Daemrich et al. 2002; Mori and Cappietti 2006; Kubowicz-Grajewska 2017) and concrete units (Kimura et al. 2002; Melito and Melby 2002; Teh 2014), as well as smooth, impermeable structures (Wang et al 2006; Koraim et al. 2014; Mahmoudof and Hajivalie 2021), which all demonstrate different behaviors. The EU-funded projects CLASH and DELOS (Vidal and Gironella 2003) generated a large database on submerged structures and many authors used this data to develop new formulae for predicting wave transmission and reflection. These formulae were later incorporated into artificial neural networks, ANNs (van Oosten 2007), which were used to predict the hydraulic performance of a range of different structures under various wave conditions. The current formulae used to predict wave transmission consider the main wave characteristics and relevant structural parameters involved in the wave transmission phenomenon (Van der Meer 1990, D'Angremond et al. 1996, Briganti et al. 2003), and other parameters that affect the hydraulic performance, such as the roughness of the armour layer, the permeability of the mound (Kurdistani et al. 2021) and the angle of the wave attack (van der Meer et al. 2005). A comprehensive review on formulae for wave transmission at submerged and low-crested breakwaters has been presented by Brancasi et al. (2022). Among the developed formulae, Goda and Ahrens (2008) provided a formula for the wave transmission coefficient able to differentiate the contribute of transmission due to overtopping over the structure and due to the infiltration through the structure. Later, Tomasicchio and D'Alessandro (2013) re-calibrated this formula on a larger database. As said, the use of submerged breakwaters has been typically limited to areas characterized by a small and moderate tidal range, so there is a lack of technical literature regarding the performance of such structures in the presence of large tidal ranges. In the present study, the performance of a submerged breakwater in presence of a large tidal range (e.g., larger than 2 m) has been evaluated by means of a laboratory investigation conducted at the EUMER laboratory (www.eumer.eu) of the University of Salento (Lecce, Italy). Then, the time-averaged numerical model CSHORE developed at the University of Delaware (www.coastal.udel.edu) has been calibrated with the observed data. CSHORE is a reliable

[1] Department of Engineering for Innovation, University of Salento, Lecce, 73100, Italy
[2] CWP Engineering, UAE
[3] IceBreak Consulting Engineers, Iceland
[4] Department of Civil and Environmental Engineering, University of Delaware
[5] Polytechnic University of Bari, Bari (BA), Italy

tool for separately observing the effects of over and inner flow on wave transmission so it has been used to analyze the proportion of energy dissipated due to wave breaking, to bottom friction and to porous mound. The calibrated model has been additionally used to numerically investigate the SBW performance for a broader range of wave conditions.

## LABORATORY INVESTIGATION

### Experimental setup

Physical model tests have been conducted in the 2D wave flume at the EUMER laboratory of the University of Salento (Lecce, IT). The flume is 45 m long, 1.4 m wide and 2 m deep. It is equipped with a piston-type wave generator endowed with an Active Reflection Compensation system enabling the generation and the development of regular and irregular waves. A dissipative beach has been placed at the end of the flume to minimize the induced wave reflection. In the wave flume, a bathymetry composed of 5 segments has been constructed with the following slopes: a flat segment in front of the wave generator to accommodate them; 3 approaching slopes of 1:8, 1:45 and 1:130, respectively, and another flat segment at the structure rear side (Figure 1). A 1:25 scaled model with the Froude scale of a rubble-mound submerged breakwater has been constructed with a crest width equal to 0.8 m and 1:2 front and rear slopes; the nominal diameter of the armour and core rock units are equal to 0.040 m and 0.026 m, respectively; the density of both armour and core is 2760 kg/m$^3$. The flume has been instrumented with nine (9) wave gauges: 1 Offshore (*WG,o*) to measure the wave characteristics in deep waters, 4 probes seaward the structure (Reflection Array) to measure the incident and reflected waves; 4 probes landward to the structure (Transmission Array) to measure the transmitted waves and thus assess the energy dissipation induced by the presence of the submerged structure. The decomposition of incident and reflected wave components is based on a development (HR Wallingford 2015) of the least squares method of Mansard and Funke (1980). Figure 1 shows a cross-section of the wave flume together with the bathymetry, the investigated structure and the instrumentation.

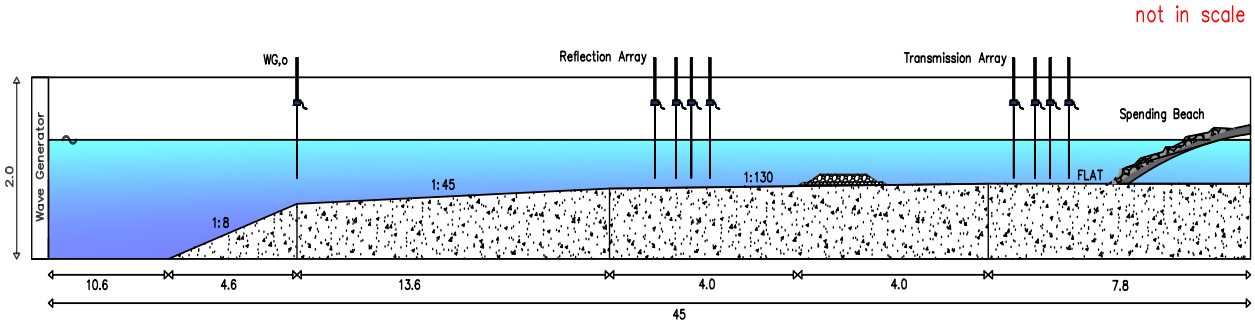


Figure 1: Definition sketch of the flume cross section

Two structure geometries have been considered with two different values of submergence (crest freeboard). The first original configuration, reported as C1, has a height of 0.14 m, while an alternative configuration, reported as C2, has an extra row of stones on the crest, resulting in a structure height of 0.18 m. Figure 2 shows the two configurations of the structure in detail.

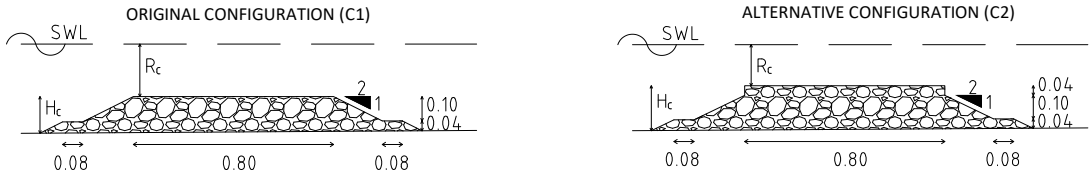


Figure 2: Original C1 (right) and alternative C2 (left) configurations of the experimental small scale submerged breakwater

Ten combinations of irregular wave conditions at *WG,o* and water levels have been tested in C1 configuration. Of these, only a number of combinations has also been tested in C2 configuration. The duration of wave attacks has been defined considering the time required to simulate a statistically reliable sea state (about 1000 waves) (Frostick et al. 2011). Table 1 summarizes the duration, the wave

characteristics in the experiments at *WG,o*, defined by the energy-based wave height, $H_{m0}$, and the wave peak period, $T_p$, (purged of the reflection component) together with the crest freeboard (i.e., the distance from the free surface to the crest of the structure, see Figure 2), $R_c$, the wave steepness at *WG,o*, $s = \frac{2\pi}{g}\frac{H_{m0}}{T_p^2}$, and the relative crest freeboard, defined as the ratio $R_c/H_{m0}$. $R_c$ is considered negative as the structure is submerged. It is worth noting that $R_c$ has a wide variability (i.e., from -0.02m to -0.21m), confirming the condition of large tidal range.

Table 1: Observed wave characteristics, $R_c$, $s$, and $R_c/H_{m0}$ at *WG,o*

| Experimental Test | Duration [s] | $H_{m0}$ [m] | $T_p$ [s] | $R_c$ [m] | s [-] | $R_c/H_{m0}$ [-] |
|---|---|---|---|---|---|---|
| **C1-1** | 1300 | 0.05 | 1.3 | -0.21 | 0.02 | -3.96 |
| **C1-2** | 1800 | 0.04 | 1.8 | -0.21 | 0.01 | -5.78 |
| **C1-3** | 2600 | 0.13 | 2.6 | -0.21 | 0.01 | -1.65 |
| **C1-4** | 2600 | 0.12 | 2.6 | -0.10 | 0.01 | -0.77 |
| **C1-5** | 2600 | 0.12 | 2.6 | -0.06 | 0.01 | -0.48 |
| **C1-6** | 3000 | 0.16 | 3.0 | -0.21 | 0.01 | -1.33 |
| **C1-7** | 3000 | 0.16 | 3.0 | -0.10 | 0.01 | -0.62 |
| **C1-8** | 3000 | 0.16 | 3.0 | -0.06 | 0.01 | -0.38 |
| **C1-9** | 2600 | 0.13 | 2.6 | -0.20 | 0.01 | -1.55 |
| **C1-10** | 3000 | 0.16 | 3.0 | -0.20 | 0.01 | -1.24 |
| **C2-3** | 2600 | 0.13 | 2.6 | -0.17 | 0.01 | -1.35 |
| **C2-5** | 2600 | 0.12 | 2.6 | -0.02 | 0.01 | -0.18 |
| **C2-6** | 3000 | 0.16 | 3.0 | -0.17 | 0.01 | -1.09 |
| **C2-8** | 3000 | 0.16 | 3.0 | -0.02 | 0.01 | -0.14 |
| **C2-9** | 2600 | 0.13 | 2.6 | -0.16 | 0.01 | -1.25 |
| **C2-10** | 3000 | 0.16 | 3.0 | -0.16 | 0.01 | -1.00 |

## Experimental results

The performance of the structure is directly related to the transmission coefficient as it can be used to evaluate how effective the breakwater is at attenuating the wave energy passing over and through it. In the present study, the effects of the submerged breakwater on wave transformation have been studied and quantified in terms of incident and transmitted wave characteristics. Table 2 lists the wave characteristics (purged of the reflection component) observed at the Reflection ($H_{m0,refl}$ , $T_{p,refl}$) and Transmission ($H_{m0,tra}$ , $T_{p,tra}$) Arrays, respectively, from which the observed transmission coefficient, $K_{t,obs}$, has been calculated as the ratio of incident wave height to the transmitted one.

Table 2: Observed wave characteristics at Reflection and Transmission Arrays and $K_{t,obs}$

| | Observed Incident Conditions (Reflection Array) | | Observed Transmitted Conditions (Transmission Array) | | |
|---|---|---|---|---|---|
| Experimental Test | $H_{m0,refl}$ [m] | $T_{p,refl}$ [s] | $H_{m0,tra}$ [m] | $T_{p,tra}$ [s] | $K_{t,obs}$ |
| **C1-1** | 0.047 | 1.37 | 0.042 | 1.39 | 0.89 |
| **C1-2** | 0.034 | 1.88 | 0.031 | 1.85 | 0.91 |
| **C1-3** | 0.127 | 2.70 | 0.109 | 2.65 | 0.86 |
| **C1-4** | 0.114 | 2.61 | 0.067 | 2.57 | 0.59 |
| **C1-5** | 0.113 | 2.69 | 0.049 | 2.70 | 0.43 |
| **C1-6** | 0.161 | 3.24 | 0.130 | 3.40 | 0.81 |
| **C1-7** | 0.127 | 3.14 | 0.069 | 2.87 | 0.54 |
| **C1-8** | 0.119 | 3.13 | 0.052 | 3.10 | 0.44 |
| **C1-9** | 0.128 | 2.69 | 0.110 | 2.67 | 0.86 |
| **C1-10** | 0.160 | 3.19 | 0.125 | 3.40 | 0.78 |
| **C2-3** | 0.132 | 2.66 | 0.108 | 2.70 | 0.82 |
| **C2-5** | 0.107 | 2.74 | 0.034 | 2.70 | 0.32 |
| **C2-6** | 0.160 | 3.08 | 0.125 | 3.23 | 0.78 |
| **C2-8** | 0.115 | 2.98 | 0.039 | 3.06 | 0.34 |
| **C2-9** | 0.131 | 2.74 | 0.103 | 2.74 | 0.79 |
| **C2-10** | 0.160 | 3.30 | 0.119 | 3.30 | 0.74 |

Based on the observation, $K_{t,obs}$ ranges between 0.32 and 0.91, with lower values observed as the submergence decreases, demonstrating a considerable dissipating effect on waves. Tests C2-5 and C2-8 with the highest crest freeboard, result in a lower transmission coefficient of 0.32 and 0.34, respectively. It is evident that the water depth plays a major role in energy transmission, but the incident wave conditions also have a significant impact, in fact, considering the tests with the same submergence, the wave transmission decreases as the wave height and peak period increase.
Moreover, the submerged breakwater has noted to produce, albeit slight, a dissipating effect on waves even in the tests C1-1 and C1-2 where the maximum submergence and the minimum wave height led to a condition whereby the wave breaking is not induced.

## NUMERICAL MODEL

### Model description

A numerical model has been used to predict the mean and standard deviation of the free surface elevation and to evaluate numerically the wave transmission through and over the SBW.
CSHORE is a cross-shore, (i.e., cross-sectional), numerical model initially developed by Kobayashi and Johnson (1998) to predict the cross-shore transformation under irregular nonlinear waves. The latest version of CSHORE includes the various features added over the years to the initial model and the latest updates are summarized in Kobayashi (2016).
The components of CSHORE for normally incident waves and along-shore uniformity include:

- a combined wave and current model based on time-averaged continuity, momentum, wave energy or action, and roller energy equations;
- a sediment transport model for bed load and suspended load coupled with the continuity equation of bottom sediment (which has not been used in this study)

Among the capabilities added in recent years, a relevant feature for the present study concerns the extension of the hydrodynamic model that allows to model the wet and dry zones on a permeable bottom for the prediction of wave transformation over and through a rubble mound structures (Kobayashi et al. 2007). In the permeable layer model, the vertically-integrated continuity equation relates the volume flux per unit width with water flux inside the permeable layer, resulting in a combined wave overtopping rate above and through the permeable layer. The momentum equation for the case of alongshore uniformity is here reported:

$$\frac{d}{dx}\left[\frac{E}{\omega}\left(C_g \cos\theta + \frac{Q_x}{\bar{h}}\right)\right] = -\frac{D_B + D_f + D_p}{\omega} \tag{1}$$

where $E$ is the specific wave energy, ω is the intrinsic angular frequency, $C_g$ is the group velocity, θ is the incident angle relative to the shore normal, $Q_x$ is the water flux in $x$ direction and $\bar{h}$ is the mean water depth. The specific wave energy is dissipated along the x-axes due different contributions: $D_B$, $D_f$ and $D_p$ which are the wave energy dissipation rate per unit horizontal area due to wave breaking, to bottom friction and to flow resistance in the permeable layer, respectively.
The energy dissipation rate $D_B$ due to wave breaking is estimated using the formula by Battjes and Stive (1985), modified to account for the local bottom slope and to extend the computation to the lower swash zone as follows:

$$D_B = \frac{\rho g a_s Q H_B^2}{4T} \tag{2}$$

Where $\rho$ is the water density, $g$ is the acceleration due to the gravity, $a_s$ is the slope effect parameter, $Q$ is the fraction of breaking waves, $H_b$ is the breaker wave height and $T$ is the intrinsic wave period.
The energy dissipation due to the bottom friction depends on the bottom friction factor, $f_b$, the depth-averaged cross-shore velocity, $\overline{U_a}$, and is expressed as:

$$D_f = \frac{1}{2}\rho f_b \overline{U_a^3} \tag{3}$$

The energy dissipation rate due to flow resistance in the permeable layer is expressed as a function of the laminar and turbulent flow resistance coefficients, $\alpha_p$ and $\beta_p$, the instantaneous cross-shore and longshore discharge velocities, $U_p$ and $V_p$, and the thickness of the permeable layer, $H_p$, as follows:

$$D_p = \rho h_p \left[\alpha_p\left(\overline{U_p^2 + V_p^2}\right) + \beta_p\left(\overline{U_p^2 + V_p^2}\right)^{1.5}\right] \tag{4}$$

The formulas for $\alpha_p$ and $\beta_p$ have been proposed by van Gent (1995) as follows

$$\alpha_p = \alpha_0 \frac{\left(1-n_p\right)^2}{n_p^2}\frac{v}{D_{n50}^2} \qquad \beta_p = \beta_1 + \frac{\beta_2}{\sigma_p} \tag{5}$$

with:

$$\beta_1 = \frac{\beta_0\left(1-n_p\right)}{n_p^3 D_{n50}} \qquad \beta_2 = \frac{7.5\beta_0\left(1-n_p\right)}{\sqrt{2}n_p^2 T} \tag{6}$$

where $\alpha_0$ and $\beta_0$ are the empirical parameters calibrated as $\alpha_0 = 1000$ and $\beta_0 = 5$ (Kobayashi 2007), $n_p$ is the porosity of the permeable layer consisting of stone, $v$ is the kinematic viscosity of the fluid and $D_{n50}$ is the nominal stone diameter.

### Model calibration

The model has been preliminary calibrated considering a numerical domain including the 3 sloping segments and the flat segment at the rear side of the structure, as shown in the Figure 3. The origin of the domain is placed at the *WG,o* along the x-axis and at SWL (Still Water Level) along the z-axis. The picture is not scaled along the x-axis to allow a better visualization of distances from the origin of the domain and to better visualize the structure.

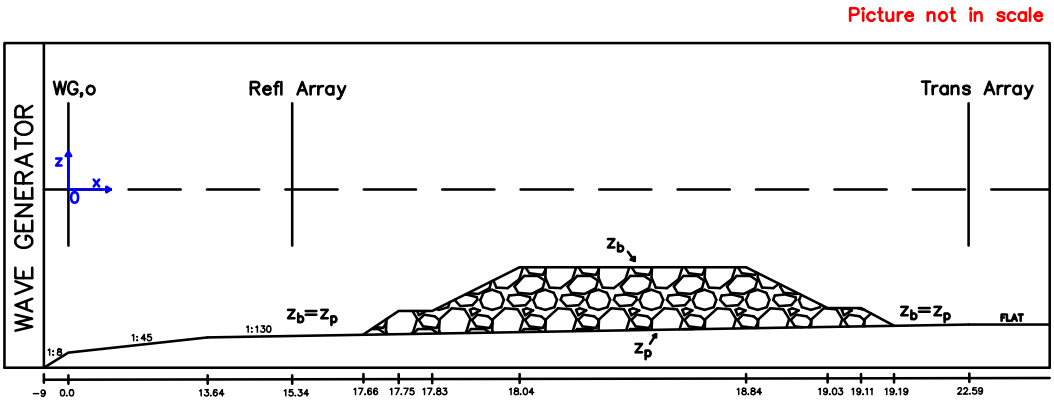


Figure 3: Sketch of numerical domain division

The $D_{50}$ of the armour layer used in the experimental tests, equal to 0.04m, has been implemented in the numerical model. The elevations of the impermeable and permeable layer are defined by $z_p$ and $z_b$, respectively, whose difference represents the thickness of the permeable layer, $H_p$; outside the structure, the two layers overlap. The impermeable layer, composed of concrete, has a bottom friction factor equal to 0. All experimental tests have been used to calibrate the model (i.e., C1 and C2 test series). The wave conditions used as input are those listed in Table 1 at *WG,o*. The calibration process involved the parameters related to all dissipation contributions, as reported in Table 3.

Table 3: Parameters involved in the calibration process

| Symbol | Parameter | Related dissipation | Starting value | Variability range |
|---|---|---|---|---|
| $\gamma$ | Breaking parameter | $D_b$ | 0.7 | (0.6 – 0.7) |
| $f_w$ | Friction factor (on the structure) | $D_f$ | 0.01 | (0.005 – 0.05) |
| $\alpha$ | Permeable layer coefficients | $D_p$ | 1000 | (100 – 1500) |
| $\beta$ | | $D_p$ | 5 | (1 – 10) |

The breaking parameter $\gamma$ related to the dissipation due to wave breaking, whose standard value is equal to 0.7, has been varied between 0.6 and 0.7; the friction factor $f_w$ on the structure related to dissipation rate due to the bottom friction, which reports a typical value of 0.01 (Cox and Kobayashi 1997), has been varied between 0.005 and 0.05; finally, the values of $\alpha$ and $\beta$ related to the dissipation due to the permeable layer of the structure, which have been previously calibrated at 1000 and 5 (Kobayashi et al. 2007), have been varied between 100 and 1500 and 1 and 10, respectively. Calibration has been carried out for one parameter at a time: one parameter has been varied at a time, with the remaining ones unchanged. Model performance has been evaluated by comparing the observed transmission coefficients and the calculated ones with the numerical model. The degree of agreement between the observed and calculated values has been quantified by means of a statistical parameter, the RMSE (root means square error), defined as:

$$RMSE = \sqrt{\frac{\sum\left(k_{t,comp} - k_{t,obs}\right)^2}{\sum k_{t,obs}^2}} \tag{7}$$

where $k_{t,comp}$ and $k_{t,obs}$ are the computed and observed wave transmission coefficients, respectively. Generally, the best value of each parameter in the calibration process is determined by selecting the one that lead the lowest sum of RMSE ($\sum RMSE$) for C1 and C2 test series.
Figure 4 shows $k_{t,comp}$ and $k_{t,obs}$ as a function of $f_w$ = 0.005, 0.01 and 0.05. It is worth noting that $f_w$ = 0.05 leads to a large $\sum RMSE$, resulting in a condition to be avoided. Theoretically, the lowest $\sum RMSE$ is obtained for $f_w$ = 0.005; however, this would lead to a deviation from the line of perfect agreement of some tests with large $k_{t,obs}$. From these considerations, $f_w$ has been assumed equal to 0.01, in agreement with the results from others studies (Cox and Kobayashi 1997).

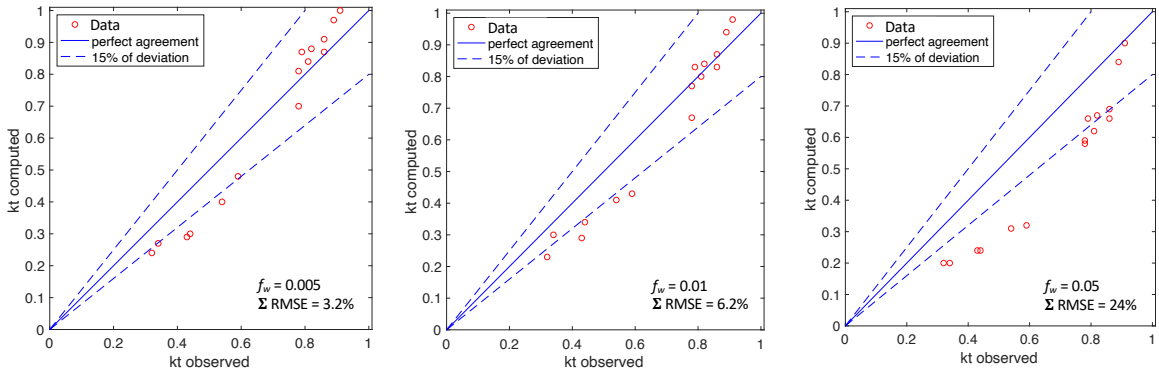


Figure 4: $k_{t,comp}$ and $k_{t,obs}$ of C1 and C2 test series as a function of $f_w$ = 0.005, 0.01 and 0.05

Then, the breaking parameter $\gamma$ has been calibrated while keeping the other parameters constant. As shown in Figure 5, the typical value $\gamma = 0.7$ provides the lowest $\sum RMSE$.

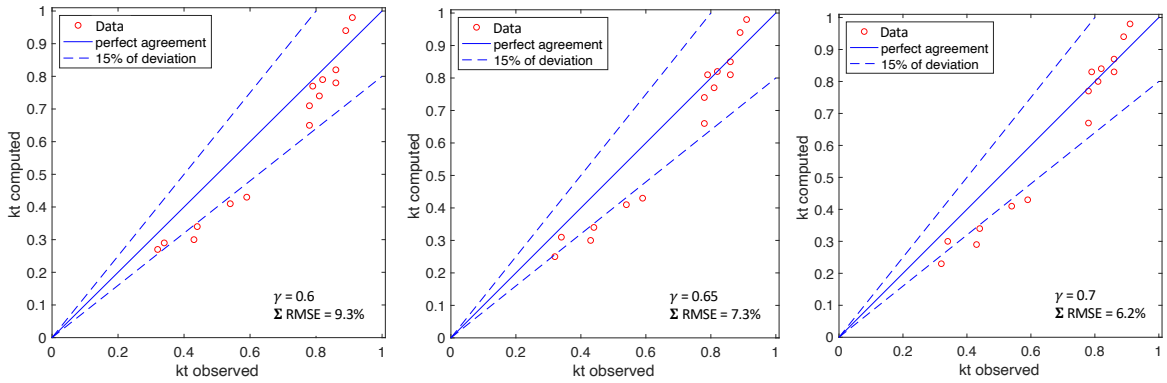


Figure 5: $k_{t,comp}$ and $k_{t,obs}$ of C1 and C2 test series as a function of $\gamma = 0.6$, 0.65 and 0.7

Finally, a number of combinations of $\alpha$ and $\beta$ has been considered. Under similar conditions, Kobayashi (2007) calibrated these parameters as $\alpha = 1000$ and $\beta = 5$. Table 4 list the $\sum RMSE$ as a function of $\alpha$ and $\beta$ for the present experimental data. It has been observed that a number of combinations lead the lowest $\sum RMSE = 5.6$., thus leaving the choice to use the first useful combination of $\alpha = 750$ and $\beta = 3$, in fact, by increasing these values, the result does not improve in terms of $\sum RMSE$.

Table 4: sum of RMSE [m] for C1 and C2 test series as a function of $\alpha$ and $\beta$

| $\sum RMSE$ | $\alpha$ = 500 | $\alpha$ = 750 | $\alpha$ = 1000 | $\alpha$ = 1200 | $\alpha$ = 1500 |
|---|---|---|---|---|---|
| **$\beta$ = 1** | 10.9 | 9.1 | 9.1 | 9.1 | 9.1 |
| **$\beta$ = 3** | 8.3 | 5.6 | 6.4 | 6.4 | 7.2 |
| **$\beta$ = 5** | 8.3 | 5.6 | 6.2 | 6.2 | 6.2 |
| **$\beta$ = 8** | 8.3 | 5.6 | 5.8 | 5.8 | 5.8 |
| **$\beta$ = 10** | 8.3 | 5.6 | 5.8 | 5.8 | 5.8 |

### Wave dissipation rates

The calibrated model allowed to investigate the fraction of each wave energy dissipation contribution for each test. As an example, Figure 6 shows the comparison between the computed and observed $H_{m0}$ for C1-3 and C2-8 as they refer to a condition of highest and lowest submergence, respectively (i.e., -0.21m and -0.02m); the origin along the z-axis is at the SWL, the green line corresponds to the structure, the orange line indicates the computed $H_{m0}$ along x-axis, and the black dots indicate the observed $H_{m0}$ at the two arrays; as can be seen, there is a reasonably good agreement, so the numerical model reasonably predicts the wave transformation along the flume in presence of the structure. Figure 7 shows, in the upper panel, the evolution of wave momentum (Eq.1) along the x-axis for C1-1 and C1-3: in both tests, it is evident an energy loss due to approaching the structure, a massive loss above and along the submerged structure, and finally a retention of energy on the rear side of the structure in the flat zone of the flume. The contribution of each of the dissipation rates due to wave breaking, $D_b$, friction on the structure, $D_f$, and porous mound, $D_p$, (divided by $g$ and $\rho$) is shown in the lower panel: in C1-1, the largest contribution is given by the dissipation for the permeable layer since the wave conditions do not induce wave breaking. On the contrary, in C1-3, the wave conditions are such that the contribution due to wave breaking overcomes all others.

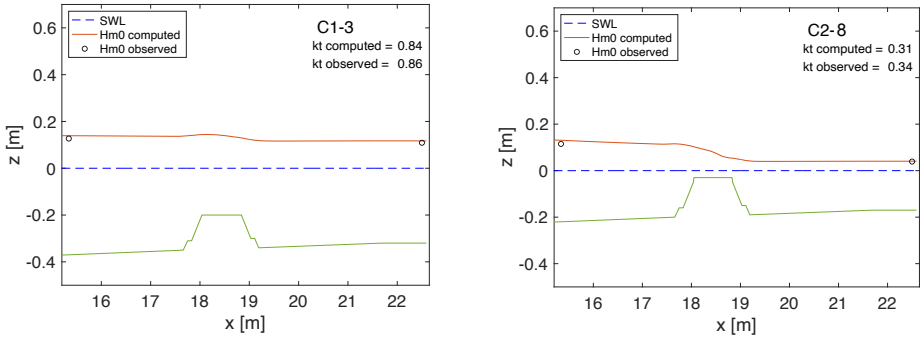


Figure 6: Comparison between observed and computed $H_{m0}$ for C1-3 and C2-8

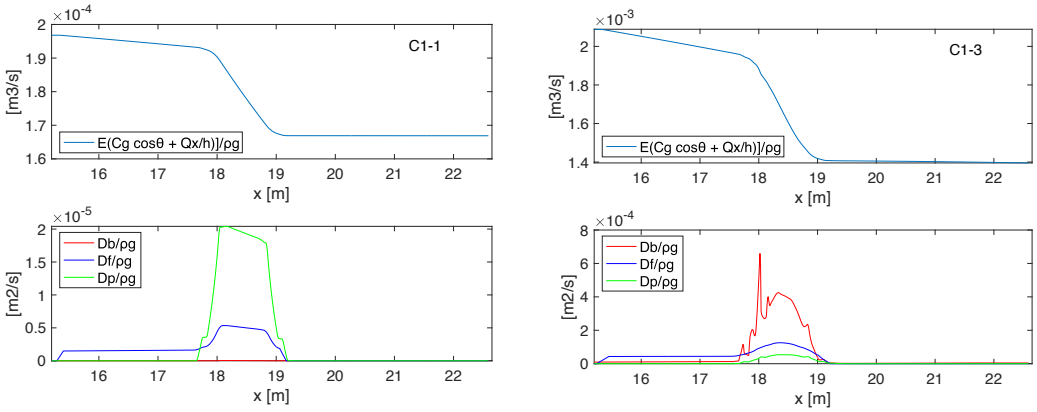


Figure 7: Wave momentum in Eq.1 (upper panel) and dissipation rates (lower panel) for C1-1 and C1-3

The maximum values of dissipation rates of all experimental tests in the two structure configurations are shown in Figure 8 as a function of the wave steepness, $s$, and the relative crest freeboard, $R_c/H_{m0}$.

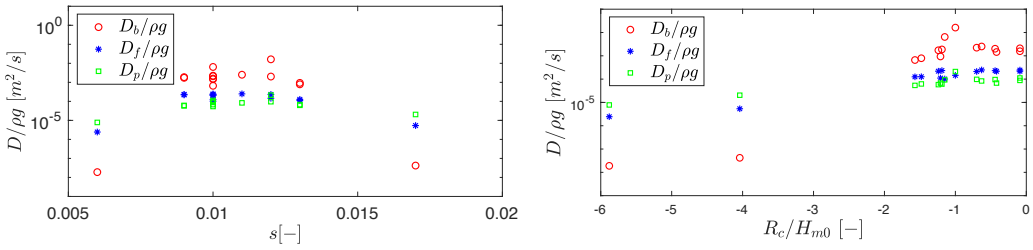


Figure 8: Maximum value of dissipation rates as a function of $s$ (right) and $R_c/H_{m0}$ (left) for C1 and C2 test series

In the plot on the right, it is evident that the wave breaking is predominant in a specific range, while two conditions can be observed in which the dissipation due to the permeable layer is prevailing; these two conditions refer to tests in which the waves are not such as to induce the wave to break (C1-1 and C1-2). In the plot on the left, two zones are noticeable: a condensation for which wave breaking is predominant on the right-hand side and an area for low values of $R_c/H_{m0}$ for which dissipation due to the permeable layer is predominant on the left-hand side.

### Additional Numerical Tests

Once the numerical model has been calibrated for the experimental tests referring to a condition of large tidal range, CSHORE has been used to simulate some additional cases, named C1-11-45, including larger tidal range. The original configuration C1 of the structure has been considered. Seven wave conditions

defined by $H_{mo}$ and $T_p$ at *WG,o* (see Figure 3) have been considered as input conditions in the numerical model, resulting in ranges of wave steepness, $s = \frac{2\pi}{g}\frac{H_{m0}}{T_p^2}$, from 0.01 to 0.07 over five values of submergence (-0.20 to -0.01 m) resulting in ranges of relative submergence from -10 to -0.05. Table 5 lists the input wave characteristics, $s$, $R_c$, and $R_c/H_{m0}$ for additional numerical tests.

Table 5: Wave characteristics, $s$, $R_c$, and $R_c/H_{m0}$ for additional numerical tests at *WG,o*

| Numerical Test | $H_{m0}$ [m] | $T_p$ [s] | s [-] | $R_c$ [m] | $R_c/H_{m0}$ [-] |
|---|---|---|---|---|---|
| C1 11 - 45 | 0.20 | 1.40 | 0.07 | -0.20 | -10.0 / -0.05 |
| | 0.15 | 1.30 | 0.06 | -0.15 | |
| | 0.10 | 1.20 | 0.04 | -0.10 | |
| | 0.08 | 1.30 | 0.03 | -0.05 | |
| | 0.06 | 1.30 | 0.02 | -0.01 | |
| | 0.04 | 1.20 | 0.02 | | |
| | 0.02 | 1.00 | 0.01 | | |

Figure 9 shows the maximum values of dissipation rates as a function of $s$ and $R_c/H_{m0}$. It is worth noting that in the panel on the left, the relative submergence equal to -2 can be referred to as the limit between low and large submergence and demarcates a change in the behavior of the phenomenon: for values below this threshold, dissipation is dominated by the permeable layer of the structure, while for higher values it is dominated by breaking. In addition, in the panel on the right, the change in behavior is visible for $s$ = 0.04 where above this threshold the behavior for all tests is the same, with a predominance of dissipation by breaking. For values below that threshold, the behavior is not unique: there is a strong dependence on the submergence (as observed in the experimental results), in fact for same values of steepness, different values of submergence provide different results.

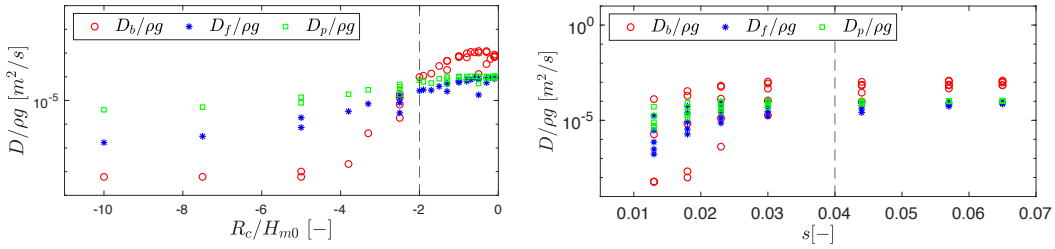


Figure 9: Maximum value of dissipation rates as a function of $s$ (right) and $R_c/H_{m0}$ (left) for C1 11 – 45 numerical tests

## CONCLUSIONS

The present research addressed the study of wave transmission and associated energy at submerged structures under conditions of large tidal range. An experimental investigation in the 2D wave flume of the EUMER Laboratory on two configurations of a small-scale submerged breakwater have been conducted under different wave conditions with large tidal range. The performance of the structure varies strongly according to the submergence of the structure and, with lower impact, to the wave conditions. An improvement in performance is observed as the water level decreases since the wave is more affected by the presence of the structure and a large amount of energy can be dissipated. By the way, the dissipative effect of the structure is noticeable even at high values of submergence: with higher values of submergence, the performance of the structure is reduced, but nevertheless its energy-dampening function remains effective. The experimental observations have been used to calibrate the numerical model CSHORE. The calibration process involved a number of parameters affecting the phenomenon of wave transmission ($\gamma$, $f_w$, $\alpha$ and $\beta$). The calibrated model allowed to investigate the fraction of each wave energy dissipation contributions among the wave breaking, the friction on the structure and the permeable layer of the structure. Finally, additional numerical tests have been carried out to cover a wider range of the dimensionless parameters $s$ and $R_c/H_{m0}$. The value $R_c/H_{m0}$ = -2 indicates the limit between low and large submergence for the cases considered in this study with a prevalence of dissipation due to breaking for values of $R_c/H_{m0}$ greater than -2 and dissipation due to the permeable layer of the structure for values less than -2. In addition, for values of $s$ greater than 0.04, wave breaking is always predominant in energy dissipation., while below that value, submergence plays a major role.

**ACKNOWLEDGMENTS**

We acknowledge the support provided by researchers at the EUropean Maritime Environmental Research (EUMER) at the University of Lecce.

**REFERENCES**

Battjes, J. A., and Stive, M. J. F. Calibration and verification of a dissipation model for random breaking waves. *Journal of Geophysical Research: Oceans* **1985**, *90*(C5), 9159-9167.

Brancasi, A., Leone, E., Francone, A., Scaravaglione, G. and Tomasicchio, G. R. On Formulae for Wave Transmission at Submerged and Low-Crested Breakwaters. *Journal of Marine Science and Engineering* **2022**, p.1986, 10(12).

Briganti, R., van der Meer, J., Buccino, M. and Calabrese, M. Wave Transmission Behind Low-Crested Structures. In *Coastal Structures* **2003**; American Society of Civil Engineers: Reston, VA, 2004; pp 580–592.

Calabrese, M., Vicinanza, D. and Buccino, M. Large-scale experiments on the behaviour of low crested and submerged breakwaters in presence of broken waves. In *Coastal Engineering* **2002**: Solving Coastal Conundrums (pp. 1900-1912).

*CLASH Project*. Available online: http://www.clash-eu.org (accessed on 6 August 2021).

Cox, D. T., and Kobayashi, N. Kinematic undertow model with logarithmic boundary layer. *J. Waterway, Port, Coastal, Ocean Eng.* **1997**, 123, 6, 354–360.

d'Angremond, K., van der Meer, J. W. and de Jong, R. J. Wave Transmission at Low-Crested Structures. In *Coastal Engineering* **1996**; American Society of Civil Engineers: New York, NY, 1997; pp 2418–2427.

Daemrich, K.-F., Mai, S. and Ohle, N. Wave Transmission at Submerged Breakwaters. In *Ocean Wave Measurement and Analysis,* **2001**; American Society of Civil Engineers: Reston, VA, 2002; pp 1725–1734.

*DELOS Project*. Available online: http://www.delos.unibo.it (accessed on 6 August 2021).

Frostick, L. E., McLelland, S. J., and Mercer, T. G. Users guide to physical modelling and experimentation, **2011**. IAHR Des. Manual.

Goda, Y. and Ahrens, J. P. New Formulation Of Wave Transmission Over And Through Low-Crested Structures. In *Coastal Engineering* **2008**; World Scientific Publishing Company, pp 3530–3541.

Johnson, B. D., and Kobayashi, N. Nonlinear time-averaged model in surf and swash zones. In *Coastal Engineering* **1998** (pp. 2785-2798).

Kimura, K., Shimizu, Y., Taya, T., Yamamoto, Y., Doi, Y. and Hanzawa, M. Characteristics of Deformation and Wave Transmission for Wide Submerged Breakwaters with Armor Blocks. In *Proc. Coastal Engineering,* **2002** *(Vol. 49, pp. 816-820),* JSCE.

Kobayashi, N. Coastal sediment transport modeling for engineering applications. *Journal of Waterway, Port, Coastal, and Ocean Engineering* **2016**, *142*(6), 03116001.

Kobayashi, N., Meigs, L. E., Ota, T., and Melby, J. A. Irregular breaking wave transmission over submerged porous breakwater. *Journal of waterway, port, coastal, and ocean engineering* **2007**, *133*(2), 104-116.

Koraim, A. S., Heikal, E. M. and Abo Zaid, A. A. Hydrodynamic Characteristics of Porous Seawall Protected by Submerged Breakwater. *Applied Ocean Research* **2014**, *46*, 1–14.

Kubowicz-Grajewska, A. Experimental Investigation into Wave Interaction with a Rubble-Mound Submerged Breakwater (Case Study). *J Mar Sci Technol* **2017**, *22* (2), 313–326.

Kurdistani, S. M., Tomasicchio, G. R., D′Alessandro, F. and Francone, A. Formula for Wave Transmission at Submerged Homogeneous Porous Breakwaters. *Ocean Engineering* **2022**, *266*, 113053.

Mahmoudof, S. M. and Hajivalie, F. Experimental Study of Hydraulic Response of Smooth Submerged Breakwaters to Irregular Waves. *Oceanologia* **2021**, *63* (4), 448–462.

Mansard, E. and Funke, E. The Measurement of Incident and Reflected Spectra Using a Least Squares Method. *Coasal Engineering* **1980**, 154–172.

Melito, I. and Melby, J. A. Wave Runup, Transmission, and Reflection for Structures Armored with CORE-LOC®. *Coastal Engineering* **2002**, *45* (1), 33–52.

Mori, E. and Cappietti, L. Wave Flume Experiments on Wave Transmission at Low Crested Breakwaters of Different Berm Width. In *Proc. IAHR-II International Short Course and Workshop on Coastal Processes and Port Engineering - SCACR*; Cosenza **2006**; pp 297–306.

Teh, H. M. Wave Transmission over a Submerged Porous Breakwater an Experimental Study. *Applied Mechanics and Materials* **2014**, *567*, 319–324.

Tomasicchio, G. R. and D'Alessandro, F. Wave Energy Transmission through and over Low Crested Breakwaters. *Journal Coastal Research* **2013**, *65*, 398–403.

van der Meer, J. W. *Data on Wave Transmission Due to Overtopping*; **1990**.

van der Meer, J. W., Briganti, R., Zanuttigh, B. and Wang, B. Wave Transmission and Reflection at Low-Crested Structures: Design Formulae, Oblique Wave Attack and Spectral Change. *Coastal Engineering* **2005**, *52* (10–11), 915–929.

van Gent, M.R.A. Porous flow through rubble-mound material. *Journal of waterway, port, coastal, and ocean engineering* **1995**, 121(3), 176-181.

van Oosten, R. P., Marco, J. P., van der Meer, J. W. and van Gent, M. R. A.; Verhagen, H. J. Wave Transmission At Low-Crested Structures Using Neural Networks. In *Coastal Engineering **2006***; World Scientific Publishing Company, 2007; pp 4932–4944.

Vidal, C. and Gironella, X. Wave Channel Experiments. Internal Report, DELOS Deliverable D32, Available from Internet. *DELOS report* **2003**.

Wallingford, H.R. Wave Gauge System: User Manual. Available online: http://equipit.hrwallingford.com/products/wave-gauges/wave-gauge-systems-8-channels (accessed on 10 September 2019).

Wang, Y. and Wang, G. Li, G. Experimental Study on the Performance of the Multiple-Layer Breakwater. *Ocean Engineering* **2006**, *33* (13), 1829–1839.